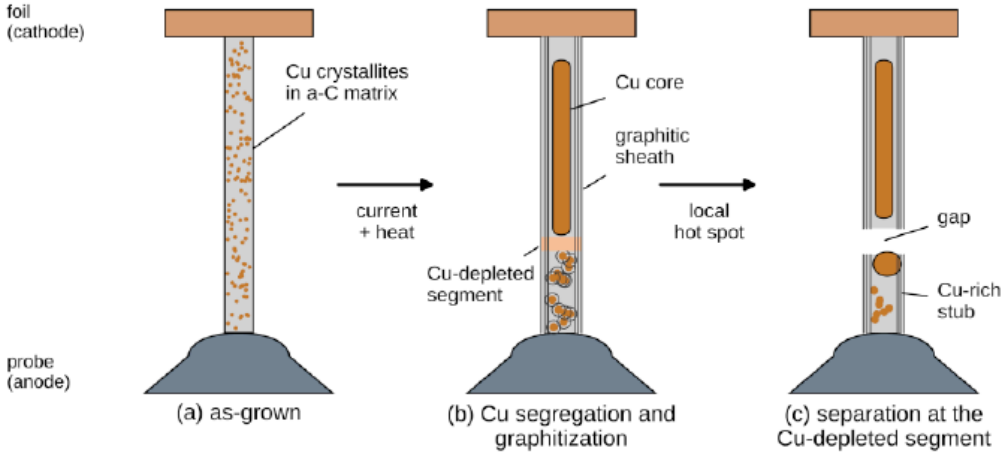
Current-Driven Restructuring of Ion-Induced Cu-Incorporated Carbon Nanofibers: In Situ TEM Observation and Electro-Thermal Analysis

Mohd Zamri Mohd Yusop[1,*] and Masaki Tanemura[2]

[1]*Faculty of Mechanical Engineering, Universiti Teknologi Malaysia, 81310 UTM Johor Bahru, Johor, Malaysia*

[2]*Department of Physical Science and Engineering, Nagoya Institute of Technology, Gokiso-cho, Showa-ku, Nagoya 466-8555, Japan*

Graphical Abstract



Abstract: In this study, we observed the structural change of a Cu-incorporated carbon nanofiber (Cu-CNF) under current flow by in situ transmission electron microscopy (TEM), and estimated the power needed for the change using an electro-thermal model. The Cu-CNFs were grown on the edge of a Cu foil by Ar^+ ion irradiation at room temperature. The selected-area electron diffraction (SAED) rings of the as-grown fiber gave d-spacings of 0.2087, 0.1808, 0.1282 and 0.1095 nm, indexed to fcc Cu with no separate graphite reflection. Under a constant bias, no structural change was observed for the first 2.0 s. Between 2.0 and 2.8 s, the fine Cu crystallites agglomerated into a continuous core of about 1.5 μm in length and 60–120 nm in width, and the surrounding carbon transformed into graphitic layers with an interlayer spacing of about 0.38 nm. At 3.2 s, the fiber broke at a Cu-depleted segment about 0.5 μm above the probe. A one-dimensional steady-state heat conduction model showed that 12–390 μW is required to heat the fiber to 600–800 °C, whereas the nominal circuit (200 mV, 200 kΩ, up to 1 μA) supplies 0.2 μW or less. The model also suggests that the heating concentrates in the Cu-free segment once a Cu core forms, which can explain the breaking point. The results indicate that the power actually delivered to the fiber was higher than the nominal value, or that a non-thermal process, such as electron-beam irradiation, assisted the change. These two cases could not be separated, because the voltage across the fiber was not recorded. The finding can be significant for designing in situ electrical processing of metal–carbon nanofibers.

Keywords: Carbon nanofiber, In situ TEM, Joule heating, Graphitization, Electro-thermal model.

1. INTRODUCTION

Graphitic carbons such as carbon nanotubes (CNTs), carbon nanofibers (CNFs) and graphene are usually synthesized at high temperature with a metal catalyst. For example, large-area graphene is grown by chemical vapor deposition (CVD) on Cu at about 1000 °C [1, 2]. Recently, several methods that heat the carbon directly have been reported. Luong *et al*. converted amorphous carbon feedstocks into turbostratic graphene within milliseconds by flash Joule heating [3]. Barreiro *et al*. transformed amorphous carbon bridges into graphene by current-induced annealing [4], and Huang *et al*. graphitized a carbon support while forming metal nanoparticles by rapid Joule heating [5]. Microwave plasma can also convert waste coffee grounds into graphene-sheet fibers [6]. From the mechanical engineering point of view, these methods are heat transfer problems. The structure obtained depends on where the heat is generated, how fast the heat escapes through the contacts, and whether the current also moves atoms, as in the electromigration of metal interconnects [7, 8].

*Address correspondence to this author at the Faculty of Mechanical Engineering, Universiti Teknologi Malaysia, 81310 UTM Johor Bahru, Johor, Malaysia;
E-mail: zamriyusop@utm.my

Received on 09-09-2026 Accepted on 26-10-2026 Published on 02-11-2026

E-ISSN: 2409-9848/26

In situ TEM with a movable nanoprobe is a useful tool to study such processes, because current can be applied to a single nanostructure during observation. Chen *et al*. reported that a high bias crystallized the walls of multiwalled CNTs and removed the outer walls [9]. Mølhave *et al*. followed the breakdown of individual CNTs by Joule heating [10], and Begtrup *et al*. and Vincent *et al*. showed that CNTs can be heated to 2000 K and above by the current [11, 12]. Regan *et al*. used the current to move metal along CNTs [13]. Using the same approach, field emission from individual pristine and N-doped graphene was measured [14], and Cu-assisted graphene growth from Cu-coated CNFs [15], Y-junction formation by electromigration-induced soldering [16] and Mo-catalyzed graphitization of amorphous carbon [17] were observed.

Ion irradiation is a simple method to grow CNFs at room temperature. A single CNF grows on the tip of each sputtered cone [18], and single ion-induced CNFs have been tested electrically, for example as field emitters across gaps below 100 nm [19]. When the cones are formed on a Cu substrate, Cu is taken into the fibers, and the CNFs become composites of fine Cu crystallites dispersed in amorphous carbon [20]. We have demonstrated that such Cu-incorporated CNFs (Cu-CNFs) change into Cu-filled structures covered with graphitic layers under bias [20, 21].

However, our previous reports compared only the structures before and after the bias, and the temperature was estimated using a simplified expression [21]. These results raise the following questions. How does Cu move from the dispersed state to the final structure? Is the electrical power supplied by the circuit large enough to heat the fiber to the graphitization temperature? Where, and why, does the fiber fail? Hence, a time-resolved observation combined with an energy balance of the whole circuit is needed.

In this study, we investigated the structural change of a Cu-CNF under current flow using the frame sequence recorded by in situ TEM. We re-indexed the SAED rings of the as-grown fiber by radial analysis and measured the structure after the current flow. We then built a one-dimensional electro-thermal model of the fiber bridged between the Cu foil and the probe. The model showed that the nominal circuit supplies at least 60 times less power than needed for graphitization. We also discuss the limitations of this interpretation, including the possible contribution of electron-beam irradiation. The results provide useful information on the power window for current-driven graphitization of metal–carbon nanofibers.

2. METHODOLOGY

2.1. Synthesis of Cu-CNFs

We used a Kaufman-type ion gun (Iontech Inc., model 3-1500-100FC) for growing the Cu-CNFs. Commercially available Cu foils with a size of 5 mm × 10 mm × 100 μm were used as substrates. A graphite plate (15 mm × 10 mm × 1 mm) was placed horizontally next to the Cu foil as a C supply. The edge of the Cu foil and the graphite plate were co-irradiated with Ar^+ ions at 45° from the normal to the surface for 45 min at room temperature [21]. The ion beam diameter and energy were 6 cm and 1 keV, respectively. The basal and working pressures were 1.5×10^{-5} and 2.0×10^{-2} Pa, respectively. It should be noted that only a single CNF grew on each cone, and no CNF grew without cone bases [21]. The morphology was examined by SEM (JEOL JSM-5600).

2.2. In Situ TEM Observation

In situ TEM observation was carried out on 24 February 2010 using a JEOL JEM-2010 operated at 200 kV at Nagoya Institute of Technology. The Cu foil was cut into a 2 mm width and directly mounted on the TEM specimen holder (JEOL; EM-Z02154T) without any post-treatment. The holder was equipped with a piezo-controlled tungsten (W) nanoprobe coated with gold (Au). The nanoprobe was slowly moved by a piezo driver to touch the tip of a single Cu-CNF. This contact also stopped the vibration of the fiber caused by charging under the electron beam [21]. The Cu foil was grounded and acted as the cathode, and the nanoprobe acted as the anode (Figure **1**). A constant bias voltage of 200 mV was applied with an external resistor R_s of 200 kΩ, which was connected in series to protect the fiber tip from current surges. The current flow was up to 1 μA [21]. The pressure in the specimen chamber was about 10^{-5} Pa. During the bias, the fiber was observed at ×30,000 with the electron beam intensity reduced to a minimum, and the images were recorded continuously with a CCD camera. The total time from the start of the bias to the breaking of the fiber was about 3.2 s. The voltage across the fiber and the current were not recorded as a function of time. Hence, the nominal values above were used in the analysis. SAED patterns were recorded at a camera length of 30 cm, and high-resolution TEM (HRTEM) images were taken before and after the bias.

2.3. Image Analysis

All measurements were carried out on the original image files using Python (NumPy and SciPy). The lengths were calibrated with the scale bar of each image. For the SAED rings of the as-grown fiber, the center of the pattern was determined from the sharpest

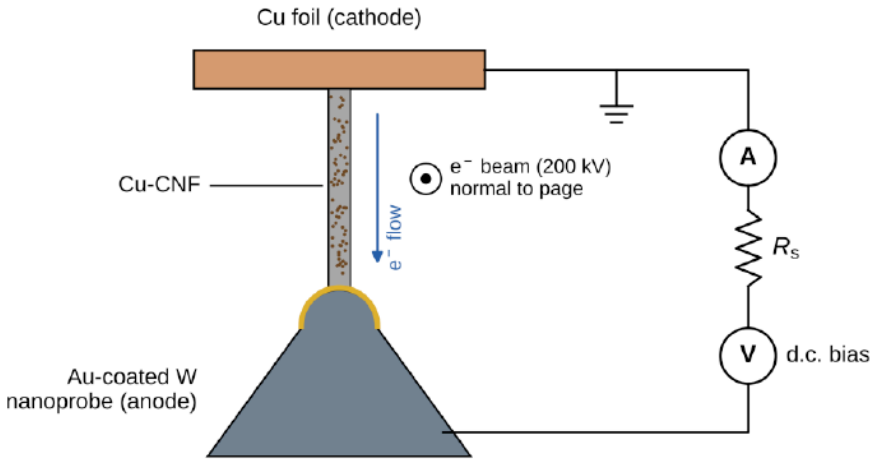


Figure 1: Schematic of the in situ TEM setup. The Cu foil with the Cu-CNF is grounded (cathode), and the Au-coated W nanoprobe is the anode. R_s is the series resistor. The electron beam is normal to the page.

ring, the intensity was averaged azimuthally with the beam stopper masked, and the background was subtracted. Although the camera length was 30 cm, the camera constant in image pixels was not calibrated. Hence, it was fixed by assigning the strongest ring to Cu (111), d = 0.2087 nm (JCPDS 04-0836). The radius ratios of the other rings were then used as an internal check, since these ratios do not depend on the calibration. The reference spacings of graphite were taken from JCPDS 41-1487. The interlayer spacing of the graphitic layers was measured from the intensity profile perpendicular to the layers in one HRTEM image.

2.4. Temperature Estimation

In order to understand the effect of Joule heating, we estimated the temperature of the fiber using a one-dimensional steady-state heat conduction model, following Vincent *et al*. [12]. The fiber is treated as a conductor with length L and diameter D bridged between two heat sinks, the Cu foil and the nanoprobe, both at T_0 = 300 K. The energy balance along the fiber is

$$\mathrm{d/dx}\,(kA\,dT/\mathrm{dx}) + I^2\rho(x)/A - \varepsilon\sigma p(T^4 - T_0^4) = 0,\ \mathrm{T(0) = T(L) = T_0} \quad (1)$$

where k is the thermal conductivity, $A = \pi D^2/4$ is the cross-sectional area, $p = \pi D$ is the perimeter, ρ is the electrical resistivity, I is the current, ε is the emissivity and σ is the Stefan–Boltzmann constant. Convection is neglected because the specimen is in high vacuum. For a uniform fiber with negligible radiation, Eq. (1) gives the maximum temperature rise at the middle of the fiber:

$$\Delta T_{max} = I^2\rho L^2/(8kA^2) = PL/(8kA) \quad (2)$$

where $P = I^2\rho L/A$ is the power dissipated in the fiber. The current is determined by the circuit, $I = V_s/(R_s + R_f + R_c)$, where V_s is the source voltage, R_f is the fiber resistance and R_c is the contact resistance. Whatever the fiber resistance is, the power delivered to the fiber cannot exceed

$$P_{max} = V_s^2/(4R_s) \quad (3)$$

which is reached when $R_f + R_c = R_s$. Eq. (1) was also solved by a finite-volume method with 801–1251 nodes to treat non-uniform fibers, with the radiation term linearized and iterated. The numerical and analytical solutions agreed within 0.1% for temperature rises below 400 K.

The input values are listed in Table **1**. L and D were measured from the first frame of the in situ observation (Section 3.2). Because k and ρ of an ion-induced Cu–C composite are not known, both were treated as bounded parameters. The range of k = 0.2–5 W m^{-1} K^{-1} covers the values of amorphous carbon films, 0.2–2.2 W m^{-1} K^{-1} [22], with a margin for Cu and partial graphitization. The range of ρ = 10^{-6}–10^{-1} Ω m covers the wide spread reported for amorphous carbon [23] and the lower values expected for a Cu-rich composite. A peak temperature of 873–1073 K (600–800 °C) was taken as the target. This is because the Ni-catalyzed graphitization of amorphous carbon in Ni–C nanocomposites starts between 400 and 800 °C [24], and Ni-catalyzed graphitization at CNT contacts has been carried out at 750 °C [25]. Cu has a low carbon solubility and is expected to need the upper end of this range.

The model is based on the following assumptions. (i) Heat flows only along the fiber axis, because the fiber length is more than ten times its diameter. (ii) Both ends of the fiber are held at T_0 = 300 K, because the Cu foil and the nanoprobe are much larger than the fiber. (iii) k and ρ are uniform within each segment and independent of temperature. (iv) Convection is absent, and radiation is included with ε = 0.8. Even if the whole

Table 1: Input Values of the Electro-Thermal Model

Quantity	Value	Basis
Fiber length, L	2.5 μm	Measured, Section 3.2
Fiber diameter, D	200 nm	Measured, Section 3.2
Thermal conductivity, k	0.2, 1 and 5 W m^{-1} K^{-1}	Range based on [22]
Electrical resistivity, ρ	10^{-6}–10^{-1} Ω m	Range based on [23]
Emissivity, ε	0.8	Assumed
Heat-sink temperature, T_0	300 K	Cu foil and probe
Target peak temperature	873–1073 K	[24, 25]
Segregated fiber, Figure 5(c)		
Cu-rich granular segment (0–0.45 μm)	k = 5 W m^{-1} K^{-1}, ρ = 10^{-5} Ω m	Estimated
Cu-depleted segment (0.45–0.60 μm)	k = 1 W m^{-1} K^{-1}, ρ = 10^{-3} Ω m	Estimated
Cu-core segment (0.60–2.5 μm)	k = 75 W m^{-1} K^{-1}, ρ = 10^{-7} Ω m	Cu core ≈ 25% of cross-section

fiber were at 1073 K, the radiative loss would be only about 0.09 μW, which is less than 1% of the smallest required power. (v) The electron beam is not included as a heat source in Eq. (1); its possible contribution is discussed separately in Section 3.4. The influence of k and ρ on the results is described in Section 3.4.

3. RESULTS AND DISCUSSION

3.1. Structure of the As-Grown Cu-CNF

Figure **2** shows the azimuthally averaged SAED intensity of the as-grown Cu-CNF. Four rings were observed. When the first ring was fixed at Cu (111), the other three rings were located at 0.1808, 0.1282 and 0.1095 nm (Table **2**). These values are in good agreement with Cu (200), (220) and (311) at 0.1808, 0.1278 and 0.1090 nm. The radius ratios of 1 : 1.154 : 1.628 : 1.905 also match the fcc sequence of 1 : 1.155 : 1.633 : 1.915 within 0.6%. This indicates that the crystallites in the fiber are fcc Cu. On the other hand, graphite (002) at 0.335 nm and (110) at 0.123 nm did not appear as separate peaks. Graphite (100) and (101) lie within 2–3% of Cu (111) and cannot be separated from it. Therefore, the carbon matrix of the as-grown fiber has no stacked graphitic order. This is consistent with the HRTEM and dark field images of the fibers from the same substrate, which showed Cu crystallites of a few nanometers dispersed randomly in amorphous carbon [21], and with the Cu-CNFs grown on Cu mesh [20]. It is noted that the rings labeled as C 120 and C 010 in our previous report [21] can be indexed to Cu alone.

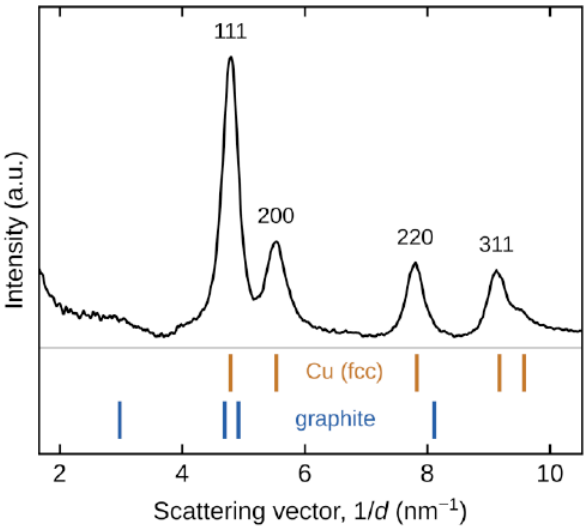


Figure 2: Azimuthally averaged SAED intensity vs. scattering vector of the as-grown Cu-CNF after background subtraction. The scattering vector is calibrated on Cu (111). The ticks mark the reference positions of fcc Cu (JCPDS 04-0836) and graphite (JCPDS 41-1487).

Table 2: Ring Spacings of the as-Grown Cu-CNF Compared with fcc Cu and Graphite

Ring	Radius ratio (measured)	Radius ratio (Cu, fcc)	d measured (nm)	Cu *(hkl), d* (nm)	Nearest graphite *(hkl), d* (nm)
1	1.000	1.000	0.2087a	111, 0.2087	100, 0.2130; 101, 0.2033
2	1.154	1.155	0.1808	200, 0.1808	–
3	1.628	1.633	0.1282	220, 0.1278	110, 0.1232 (not resolved)
4	1.905	1.915	0.1095	311, 0.1090	–

[a]Used to fix the camera constant.

3.2. Structural Change during Current Flow

Figure **3** shows the TEM images of the Cu-CNF during the current flow. In Figure **3**(**a**), the fiber touches the nanoprobe. The fiber is about 200 nm in diameter and at least 2.5 μm in length within the field of view. No structural change was observed for the first 2.0 s (Figure **3**(**a**) and 3(b)), and the difference image of the two frames stayed at the noise level. At 2.8 s (Figure **3**(**c**)), the dispersed Cu crystallites agglomerated into a continuous dark core with a length of about 1.5 μm and a width of 60–120 nm in the upper and middle parts of the fiber. On the other hand, the lower part, about 0.5 μm from the probe, contained coarse and separated particles. Between the two parts, a short bright band with little Cu contrast was formed. The fiber became wavy, and its width increased to 190–270 nm. A similar change of the fiber morphology from linear to wavy was also observed in our previous study [20]. At 3.2 s (Figure **3**(**d**)), the fiber broke at the bright band, about 0.5 μm above the probe. The upper part with the Cu core bent away from the original axis, and a round Cu-rich particle formed at the broken end of the lower part that remained on the probe. This indicates that the Cu agglomeration was completed within 0.8 s after the onset of the change, and the fiber broke within a further 0.4 s.

This result indicates that the Cu agglomeration and local Cu depletion occurred first, and the fiber broke at the Cu-depleted segment afterward. The net direction of Cu migration cannot be determined from the four frames. The continuous Cu core is located at the cathode side of the depleted band. This is consistent with the Cu agglomeration toward the cathode reported by Rosmi *et al*. for Cu-coated CNFs [15]. If electromigration by the electron wind were dominant, Cu should move toward the anode [8]. Therefore, electromigration is unlikely to be the main driving force of the Cu agglomeration at this stage, as discussed in Section 3.5.

Here, we separate what was observed from what was inferred. The observed changes are changes in the TEM contrast: the dark crystallites disappeared from the fiber within 0.8 s, a continuous dark core of about 1.5 μm appeared, and a bright band with little dark contrast formed about 0.5 μm above the probe. The dark core was identified as Cu by the spot pattern of Cu {200} in Figure **4**(**e**). The bright band was identified as Cu-depleted from its contrast alone, because energy-dispersive X-ray spectroscopy (EDS) mapping was not carried out. On the other hand, the mechanism of Cu migration is inferred. Two processes can gather fine Cu crystallites into a continuous core. The first is the coalescence of the crystallites driven by the reduction of their surface energy. The second is thermomigration of Cu along the temperature gradient. Both processes become fast only when the fiber is heated, and the heating is discussed in Section 3.4. The present data cannot separate the two processes, and EDS mapping during the bias is needed to follow the Cu distribution directly.

3.3. Structure after Current Flow

Figure **4**(**a**) shows the upper part of the fiber after the breaking. A bright carbon layer covers the Cu core along its whole length. Figure **4**(**d**) shows the HRTEM image of the outer wall. Straight graphitic layers with a thickness of a few nanometers were formed at the outer surface, and wavy few-layer sheets were formed inside. The interlayer spacing of the straight layers was 0.38 ± 0.04 nm (n = 8). This value is larger than 0.335 nm of graphite, indicating turbostratic stacking. In our previous report, a spacing of 0.34 nm was measured on a different fiber from the same substrate [21]. Both values are within the ±5% uncertainty of the uncalibrated HRTEM magnification. Figure **4**(**b**) and **4**(**c**) show the other two regions marked in Figure **4**(**a**). Closed and curved graphitic shells were formed around the remaining small particles, similar to the carbon onions formed under electron irradiation [26], and the layers along the Cu core were parallel to the Cu

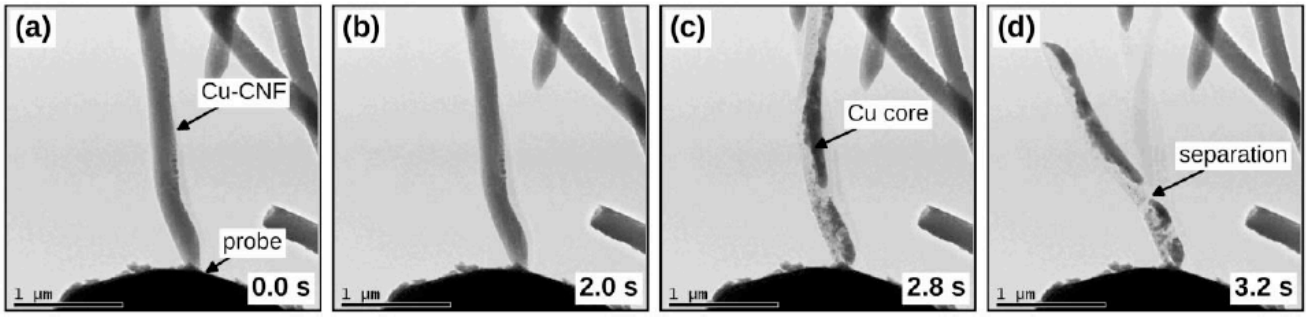


Figure 3: TEM images of the Cu-CNF during current flow. (**a**) 0.0 s, fiber in contact with the probe at the start of the bias, (**b**) 2.0 s, no structural change, (**c**) 2.8 s, Cu agglomerated into a continuous core with a Cu-depleted band near the probe and (**d**) 3.2 s, breaking of the fiber at the depleted band. Scale bars, 1 μm.

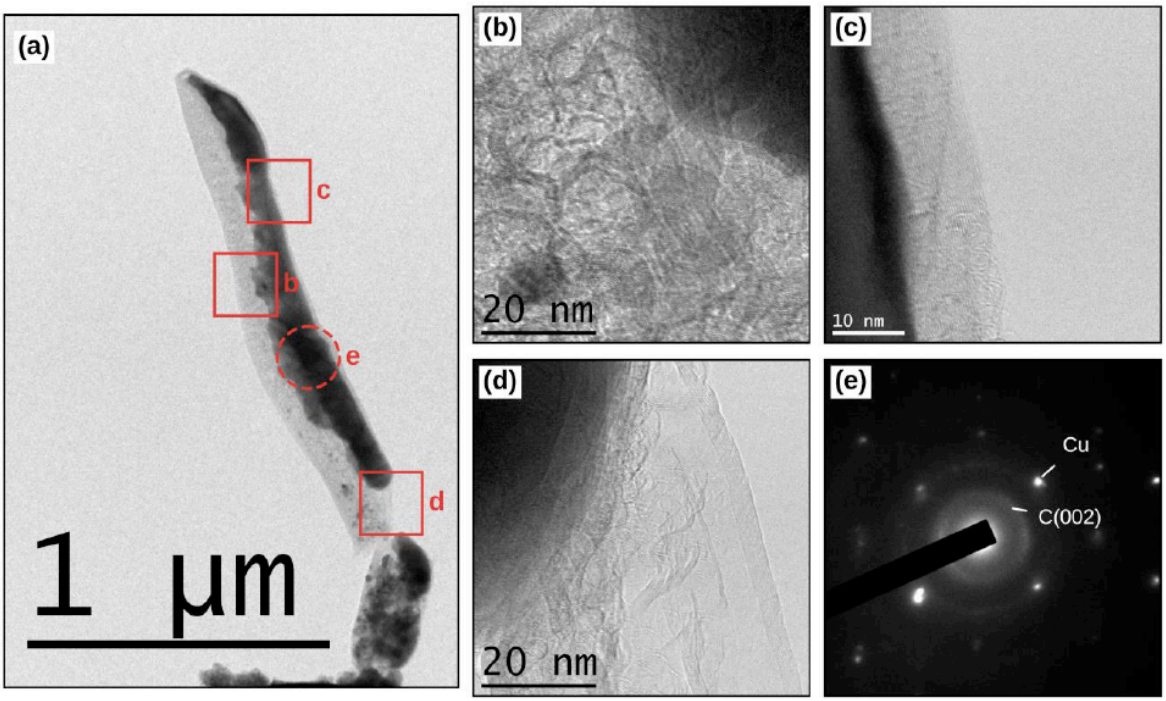


Figure 4: Structure of the Cu-CNF after current flow. (**a**) Upper part of the fiber after breaking, with the areas of (**b**)–(**e**) marked, (**b**) curved graphitic shells around the remaining particles, (**c**) graphitic layers parallel to the surface of the Cu core, (**d**) straight graphitic layers at the outer wall with wavy few-layer sheets inside (interlayer spacing 0.38 ± 0.04 nm) and (**e**) SAED pattern of the Cu core with a diffuse ring from the graphitic layers.

surface. This suggests that the graphitic layers grew on the Cu surface. It should be noted that the HRTEM images were taken after the bias at high magnification. Hence, the electron beam might have contributed to the curved shells and to part of the ordering in Figure **4**, and this contribution cannot be excluded with the present data.

The final structure varied from fiber to fiber. In the fiber reported in [21], Cu agglomerated into sphere-like single crystalline particles covered with graphitic layers of 10–13 nm, whereas a long Cu core was formed in the present fiber. Moreover, thin layers around the particles and thick layers in the particle-free region are consistent with our previous result, where fewer than 10 layers formed around the dispersed particles and more than 80 layers formed in the particle-free region [20].

Figure **4**(**e**) shows the SAED pattern of the Cu core. The pattern consists of diffraction spots, indicating that the Cu core is a single crystal or a few large grains, unlike the polycrystalline rings of the as-grown fiber. Because both SAED patterns were recorded at the same camera length of 30 cm, the camera constant of Figure **2** applies, and the strongest spots correspond to d ≈ 0.180 nm, that is, Cu {200}. The other spot pairs at d ≈ 0.194 and 0.142 nm could not be indexed to a single low-index zone axis of Cu. Together with the doubled spot near the beam stopper, this suggests overlapping domains with a small rotation. No reflection of Cu_2O (110) at 0.302 nm or (111) at 0.246 nm was observed, whereas Cu2O was found after the current flow in our previous study using a JEM-3010 [20]. A diffuse ring between 0.33 and 0.43 nm comes from the turbostratic graphitic layers, which is consistent with the measured interlayer spacing.

3.4. Temperature Estimation

Figure **5**(**a**) shows the maximum temperature rise as a function of the power dissipated in a uniform fiber. With V_s = 200 mV and R_s = 200 kΩ, Eq. (3) gives P_{max} = 50 nW. Even if the 200 mV and 1 μA are taken as the voltage and current of the fiber itself, P is 0.2 μW or less. In this case, Eq. (2) gives a temperature rise of only 10 K for k = 0.2 W m^{-1} K^{-1} and 2 K for k = 1 W m^{-1} K^{-1}. To reach 873–1073 K, P = 12–16 μW for k = 0.2, 58–78 μW for k = 1 and 290–390 μW for k = 5 W m^{-1} K^{-1} are required. This indicates that the power from the nominal circuit is 60–2000 times smaller than the required power.

Figure **5**(**b**) shows the current and the source voltage required to reach 873 K for k = 1 W m^{-1} K^{-1} over five decades of ρ. The required current is above 1 μA in the whole range. It falls to 1 μA only when ρ reaches about 0.7 Ω m, and then about 58 V is needed to drive 1 μA through the 58 MΩ fiber. With the 200 kΩ resistor, the minimum source voltage is about 7 V, which is reached when the fiber resistance equals R_s. This is more than 30 times the nominal 200 mV.

Therefore, the result does not depend on the unknown resistivity.

The two bounded parameters affect the results in different ways. From Eq. (2), the power required to reach a given ΔT_{max} is $P = 8kA\Delta T_{max}/L$. This power is proportional to k and does not depend on ρ. Hence, k sets the required power, and the lowest value, k = 0.2 W m^{-1} K^{-1}, gives the smallest estimate of 12 μW. A higher k, which is expected after graphitization or Cu agglomeration, raises the required power further. On the other hand, ρ decides how the same power is divided between the current and the voltage. For a given current, ΔT_{max} increases in proportion to ρ, whereas the current required for a given ΔT_{max} decreases in proportion to $\rho^{-1/2}$. With the series resistor, the required source voltage is smallest when $R_f = R_s$, which corresponds to $\rho \approx 2.5 \times 10^{-3}$ Ω m. Table **3** summarizes these values. In all cases, the required power is at least 60 times the nominal 0.2 μW.

We also checked two other heat sources. The first is the contact between the fiber and the probe. The spreading resistance of a contact with radius a is about 1/(4ka). For a = 2 nm and k = 1 W m^{-1} K^{-1}, this gives about 1.3×10^8 K W^{-1}, and 0.2 μW raises the contact temperature by only 25 K. The second is the electron beam. A 200 keV electron passing through 200 nm of carbon loses about 50 eV, as estimated from the inelastic mean free path and the mean energy loss per event [27]. Hence, a beam current of 1–10 nA on the fiber deposits 0.05–0.5 μW. Moreover, the beam intensity was kept at a minimum during the bias [21]. Therefore, the beam heating cannot explain the graphitization. However, 200 keV electrons exceed the knock-on threshold of carbon in graphitic networks [28], and electron irradiation alone can curl carbon into closed shells [26] and convert amorphous carbon into graphene [29]. The onion-like shells in Figure **4**(**b**) might be due to the beam, but a beam-only test on an unbiased fiber is needed to separate this effect.

Hence, steady Joule heating under the nominal condition cannot explain the observed graphitization. In this experiment, the bias was kept constant at 200 mV, and no higher bias was applied. The thermal time constant of the fiber is about 1 μs, as estimated from $L^2/(\pi^2\alpha)$ with a thermal diffusivity α of about 7×10^{-7} m^2 s^{-1}. Therefore, the fiber reaches its steady temperature within microseconds after any change of the current, and the delay of 2.0 s before the structural change cannot be explained by a slow temperature build-up. Moreover, a sudden change in TEM contrast after the start of the bias was also observed in our previous

Table 3: Influence of the Thermal Conductivity on the Required Power and Source Voltage (L = 2.5 μm, D = 200 nm)

Thermal conductivity, k (W m^{-1} K^{-1})	Required power, P (μW), 873–1073 K	ΔT_{max} at P = 0.2 μW (K)	Minimum V_s with R_s = 200 kΩ (V), 873–1073 K
0.2	12–16	9.9	3.0–3.5
1	58–78	2.0	6.8–7.9
5	290–390	0.4	15–18

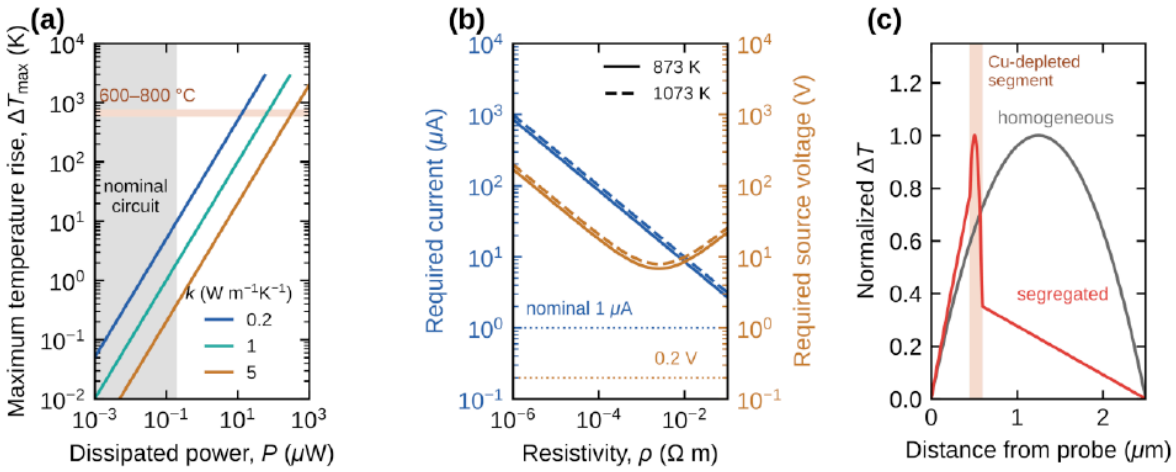


Figure 5: Results of the electro-thermal model. (**a**) Maximum temperature rise vs. power dissipated in a uniform fiber (L = 2.5 μm, D = 200 nm) for three thermal conductivities. The gray band marks the power available from the nominal circuit, and the shaded strip marks the target of 600–800 °C. (**b**) Current (left axis) and source voltage with R_s = 200 kΩ (right axis) required to reach 873 K (solid) and 1073 K (dashed) for k = 1 W m^{-1} K^{-1}. The dotted lines show the nominal 1 μA and 200 mV. (**c**) Normalized temperature profiles at 50 μA for the homogeneous fiber and the segregated fiber of Table **1**. The shaded band is the Cu-depleted segment.

study at 1 mV with a 4.5 kΩ resistor [20], where Eq. (3) gives an even smaller power of about 0.06 nW. These results indicate that either the power actually delivered to the fiber was higher than that expected from the nominal settings, or a non-thermal process assisted the change. The present data cannot separate the two cases, because the voltage across the fiber and the current were not recorded with time. Atomic displacement by the electron beam may have increased the mobility of carbon and Cu atoms, but it cannot supply the heat.

The discrepancy between the nominal power (0.2 μW or less) and the required power (12–390 μW) is the main open point of this study, and the present interpretation has the following limitations. First, the nominal bias and current were taken from the experimental conditions, and the voltage across the fiber and the current were not recorded as a function of time. Hence, the power actually delivered to the fiber could not be measured. Second, k and ρ of the Cu-CNF were not measured, and the model uses bounded values. Third, the contact resistance between the fiber and the probe, and its change during the bias, are unknown. Fourth, the electron dose on the fiber was not measured, so the non-thermal contribution of the beam cannot be estimated. Fifth, the results were obtained from a single fiber. For these reasons, the model is used here to show that the nominal conditions alone are not sufficient for thermal graphitization, and not to give the actual temperature of the fiber. The structural change is therefore not attributed solely to Joule heating. Simultaneous recording of the fiber voltage and current, beam-only tests on unbiased fibers and EDS mapping during the bias will be carried out in future work.

In our previous report, the temperature was estimated to be about 490 K [21] using the expression of Vincent *et al*. [12] for a tip of 10 nm radius, with the current confined to a single outer layer of 0.34 nm. When the same balance is applied to the measured cross-section of 200 nm, the temperature rise is only a few kelvin, and Eq. (3) limits the power to 50 nW for any conduction path. A higher power regime is supported by Rosmi *et al*., who observed graphene growth from Cu-coated CNFs at about 0.12 mA and up to 2 V using the same type of holder [15]. This power is inside the window of Figure **5**(**a**).

The present model is one-dimensional, uses constant properties and treats the electrodes as ideal heat sinks. A thermal contact resistance increases the temperature for a given power. When 10^8 K W^{-1} is added at each end, the required power decreases by a factor of 2–26 in the range of k considered. However, it is still at least about 30 times higher than the nominal power. The contact resistance between metals and carbon nanostructures strongly depends on the metal and its wettability [30]. Hence, this term should be measured in future work.

3.5. Breaking at the Cu-Depleted Segment

Figure **5**(**c**) shows the normalized temperature profiles at 50 μA for the homogeneous fiber and for the segregated fiber listed in Table **1**. In the homogeneous fiber, the maximum temperature is at the middle of the fiber. Once Cu forms a continuous core, most of the current flows through the core, and the heat generated per unit length, $I^2\rho/\mathrm{A}$, becomes small along the core. Hence, the heat generation concentrates in the Cu-free segment, where the resistivity is orders of magnitude higher, and the temperature peak moves into this segment. For the parameters in Table **1**, the Cu-depleted segment is only 6% of the fiber length (0.15 of 2.5 μm), but it carries 97% of the total fiber resistance (about 4.8 of 4.9 kΩ). The heat generated per unit length in this segment is 104 times that along the Cu core and 10^2 times that in the Cu-rich lower part. The total heating also decreases from a peak rise of 198 K to 17 K at 50 μA, because the Cu core shunts the current. This indicates that the restructuring is self-limiting except at the Cu-depleted segment. The local heating at this segment would remove more Cu and carbon and narrow the cross-section, which further increases the local heating. This feedback can be estimated with the same model. Because the 200 kΩ series resistor is much larger than the fiber resistance, the current stays almost constant when the segment becomes narrow. At 50 μA, a reduction in the diameter of the Cu-depleted segment from 200 to 160 nm raises its peak temperature rise from 17 to 34 K, and a reduction to 100 nm raises it to 157 K. This sharp increase occurs because the heat generated per unit length increases as $1/D^2$, while the heat conduction out of the segment decreases as D^2. Therefore, a small loss of material at the Cu-depleted segment accelerates the local heating, and the fiber breaks there. The narrowing itself was not resolved in the frames, because the breaking occurred within 0.4 s. A similar positive feedback causes the failure of metal interconnects by void growth under electromigration [7, 8] and the stepwise breakdown of CNTs under high current [9, 10].

On the other hand, electromigration is negligible under the nominal condition. A current of 1 μA through a Cu core of 100 nm in diameter gives about 1.3×10^4 A cm^{-2}. This is about two orders of magnitude lower than 10^6 A cm^{-2}, which is used in accelerated electromigration tests of metal lines [7, 8]. At 50–300 μA, which is needed for the heating, the current density in the Cu core reaches $0.6–4 \times 10^6$ A cm^{-2}. Therefore,

electromigration and graphitization are expected to start in the same current range. This may explain why Cu migration and graphitic restructuring were observed together in this and related studies [15-17, 20].

3.6. Proposed Model

Based on the above results, we propose a model for the structural change of the Cu-CNF under current flow, as shown in Figure **6**. Three steps are considered. The model combines the observed structural changes with the mechanisms inferred above. The driving forces in Steps 2 and 3 were not measured directly.

Step 1: Before the bias, fine Cu crystallites of a few nanometers are dispersed in the amorphous carbon matrix (Figure **6**(**a**)). The current flows through the whole cross-section, and the fiber is heated uniformly.

Step 2: When enough energy is supplied by the current flow, possibly assisted by electron-beam irradiation, the Cu crystallites coalesce into a continuous core, and the amorphous carbon around the Cu transforms into turbostratic graphitic layers parallel to the Cu surface (Figure **6**(**b**)). A short segment between the core and the lower particles is depleted of Cu.

Step 3: The Cu core shunts the current, so the heating concentrates in the Cu-depleted segment. The local temperature rise removes carbon and Cu from this segment, and the fiber breaks there (Figure **6**(**c**)).

3.7. Implications for Electrical Processing

From Eq. (2), the volumetric heating needed to raise the center of a conductor cooled at both ends by ΔT is $q^m = P/(AL) = 8k\Delta T/L^2$. When the length is halved, the required power density increases four times. This is why short nanoscale bridges between large electrodes are difficult to heat, while bulk processes such as flash Joule heating [3] reach high temperature at moderate power density. For in situ electrical processing of composite nanofibers, three practical rules are obtained. First, R_s should be chosen so that $V_s^2/(4R_s)$ exceeds the required power. With a 200 kΩ protection resistor, a source voltage of several volts is needed to heat a 2.5 μm fiber to 600–800 °C. Second, the voltage across the fiber and the current should be recorded with time, because the source setting alone does not determine the power delivered. This record was not available in the present experiment. Third, a beam-only test is needed before the structural change is attributed to Joule heating. The same rules apply to Cu–carbon nanofibers used as interconnects or nanoheaters, where Cu-depleted segments will act as hot spots and failure sites.

4. CONCLUSION

The structural change of an ion-induced Cu-CNF under current flow was observed by in situ TEM and analyzed with an electro-thermal model. The SAED rings of the as-grown fiber were indexed to fcc Cu, with no stacked graphitic order in the carbon. Under a constant bias of 200 mV, no structural change was observed for the first 2.0 s. By 2.8 s, the Cu crystallites agglomerated into a continuous core of about 1.5 μm in length, and the surrounding carbon transformed into curved and straight turbostratic layers with a spacing of about 0.38 nm. At 3.2 s, the fiber broke at a Cu-depleted segment about 0.5 μm above the probe. The model showed that 12–390 μW is needed to heat a fiber of 2.5 μm in length and 200 nm in diameter to 600–800 °C, whereas the nominal circuit supplies 0.2 μW or less. The model suggests that the heating concentrates in the Cu-free segment once the Cu core forms, which can explain the breaking point. These results indicate that the power delivered to the fiber

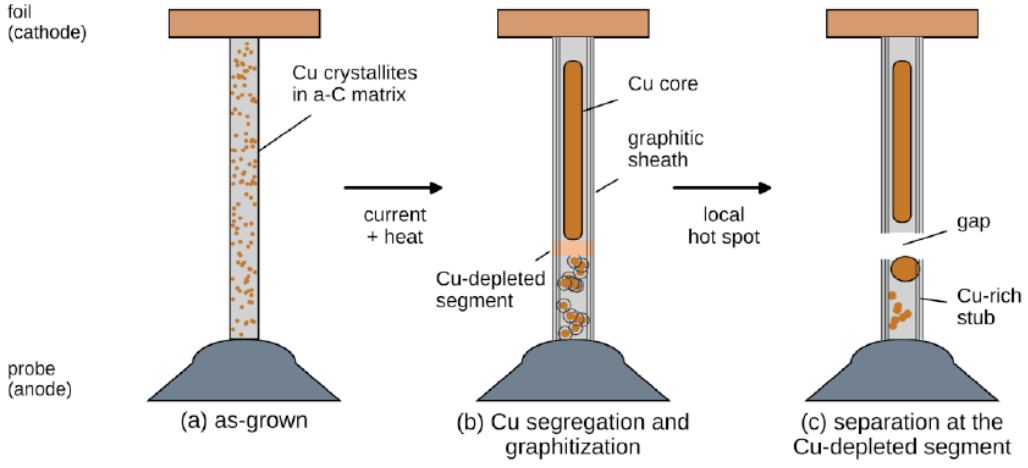


Figure 6: Proposed model for the structural change of the Cu-CNF under current flow. (**a**) Step 1: Cu crystallites dispersed in amorphous carbon, (**b**) Step 2: Cu agglomeration into a core and graphitization of the surrounding carbon, leaving a Cu-depleted segment and (**c**) Step 3: local heating and breaking at the Cu-depleted segment.

was higher than that expected from the nominal settings, or that a non-thermal process such as electron-beam irradiation assisted the change. These two cases could not be separated, because the voltage across the fiber and the current were not recorded with time. The required power density scales as $8k\Delta T/L^2$. The finding can be significant for designing the bias circuit in in situ electrical processing and for predicting hot spots in metal–carbon nanoconductors.

ACKNOWLEDGEMENT

The authors would like to thank Nagoya Institute of Technology for the use of the in situ TEM facilities.

CONFLICTS OF INTEREST

The authors declare no conflict of interest.

REFERENCES

[1] Geim, A. K. and Novoselov, K. S. 2007. The Rise of Graphene. Nature Materials. 6(3): 183-191. https://doi.org/10.1038/nmat1849

[2] Li, X., Cai, W., An, J., Kim, S., Nah, J., Yang, D., Piner, R., Velamakanni, A., Jung, I., Tutuc, E., Banerjee, S. K., Colombo, L. and Ruoff, R. S. 2009. Large-area Synthesis of High-quality and Uniform Graphene Films on Copper Foils. Science. 324(5932): 1312-1314. https://doi.org/10.1126/science.1171245

[3] Luong, D. X., Bets, K. V., Algozeeb, W. A., Stanford, M. G., Kittrell, C., Chen, W., Salvatierra, R. V., Ren, M., McHugh, E. A., Advincula, P. A., Wang, Z., Bhatt, M., Guo, H., Mancevski, V., Shahsavari, R., Yakobson, B. I. and Tour, J. M. 2020. Gram-scale Bottom-up Flash Graphene Synthesis. Nature. 577(7792): 647-651. https://doi.org/10.1038/s41586-020-1938-0

[4] Barreiro, A., Börrnert, F., Avdoshenko, S. M., Rellinghaus, B., Cuniberti, G., Rümmeli, M. H. and Vandersypen, L. M. K. 2013. Understanding the Catalyst-free Transformation of Amorphous Carbon into Graphene by Current-induced Annealing. Scientific Reports. 3: 1115. https://doi.org/10.1038/srep01115

[5] Huang, Z., Yao, Y., Pang, Z., Yuan, Y., Li, T., He, K., Hu, X., Cheng, J., Yao, W., Liu, Y., Nie, A., Sharifi-Asl, S., Cheng, M., Song, B., Amine, K., Lu, J., Li, T., Hu, L. and Shahbazian-Yassar, R. 2020. Direct Observation of the Formation and Stabilization of Metallic Nanoparticles on Carbon Supports. Nature Communications. 11: 6373. https://doi.org/10.1038/s41467-020-20084-5

[6] Wang, Z., Ogata, H., Morimoto, S., Fujishige, M., Takeuchi, K., Muramatsu, H., Hayashi, T., Ortiz-Medina, J., Mohd Yusop, M. Z., Tanemura, M., Terrones, M., Hashimoto, Y. and Endo, M. 2015. Microwave Plasma-induced Graphene-sheet Fibers from Waste Coffee Grounds. Journal of Materials Chemistry A. 3(28): 14545-14549. https://doi.org/10.1039/C5TA03833B

[7] Black, J. R. 1969. Electromigration - A Brief Survey and Some Recent Results. IEEE Transactions on Electron Devices. 16(4): 338-347. https://doi.org/10.1109/T-ED.1969.16754

[8] Ho, P. S. and Kwok, T. 1989. Electromigration in Metals. Reports on Progress in Physics. 52(3): 301-348. https://doi.org/10.1088/0034-4885/52/3/002

[9] Chen, S., Huang, J. Y., Wang, Z., Kempa, K., Chen, G. and Ren, Z. F. 2005. High-bias-induced Structure and the Corresponding Electronic Property Changes in Carbon Nanotubes. Applied Physics Letters. 87(26): 263107. https://doi.org/10.1063/1.2155116

[10] Mølhave, K., Gudnason, S. B., Pedersen, A. T., Clausen, C. H., Horsewell, A. and Bøggild, P. 2006. Transmission Electron Microscopy Study of Individual Carbon Nanotube Breakdown Caused by Joule Heating in Air. Nano Letters. 6(8): 1663-1668. https://doi.org/10.1021/nl060821n

[11] Begtrup, G. E., Ray, K. G., Kessler, B. M., Yuzvinsky, T. D., Garcia, H. and Zettl, A. 2007. Probing Nanoscale Solids at Thermal Extremes. Physical Review Letters. 99(15): 155901. https://doi.org/10.1103/PhysRevLett.99.155901

[12] Vincent, P., Purcell, S. T., Journet, C. and Binh, V. T. 2002. Modelization of Resistive Heating of Carbon Nanotubes during Field Emission. Physical Review B. 66(7): 075406. https://doi.org/10.1103/PhysRevB.66.075406

[13] Regan, B. C., Aloni, S., Ritchie, R. O., Dahmen, U. and Zettl, A. 2004. Carbon Nanotubes as Nanoscale Mass Conveyors. Nature. 428(6986): 924-927. https://doi.org/10.1038/nature02496

[14] Kashid, R. V., Yusop, M. Z., Takahashi, C., Kalita, G., Panchakarla, L. S., Joag, D. S., More, M. A. and Tanemura, M. 2013. Field Emission Characteristics of Pristine and N-doped Graphene Measured by In-situ Transmission Electron Microscopy. Journal of Applied Physics. 113(21): 214311. https://doi.org/10.1063/1.4809930

[15] Rosmi, M. S., Yusop, M. Z., Kalita, G., Yaakob, Y., Takahashi, C. and Tanemura, M. 2014. Visualizing Copper Assisted Graphene Growth in Nanoscale. Scientific Reports. 4: 7563. https://doi.org/10.1038/srep07563

[16] Sharma, S., Rosmi, M. S., Yaakob, Y., Yusop, M. Z. M., Kalita, G., Kitazawa, M. and Tanemura, M. 2018. In Situ TEM Synthesis of Carbon Nanotube Y-junctions by Electromigration Induced Soldering. Carbon. 132: 165-171. https://doi.org/10.1016/j.carbon.2018.02.037

[17] Sharma, S., Jaisi, B. P., Araby, M. I., Elnobi, S., Ayhan, M. E., Kalita, G. and Tanemura, M. 2019. The Mo Catalyzed Graphitization of Amorphous Carbon: An In Situ TEM Study. RSC Advances. 9(59): 34377-34381. https://doi.org/10.1039/C9RA05936A

[18] Tanemura, M., Okita, T., Yamauchi, H., Tanemura, S. and Morishima, R. 2004. Room-temperature Growth of a Carbon Nanofiber on the Tip of Conical Carbon Protrusions. Applied Physics Letters. 84(19): 3831-3833. https://doi.org/10.1063/1.1745109

[19] Sim, H. S., Lau, S. P., Ang, L. K., You, G. F., Tanemura, M., Yamaguchi, K., Zamri, M. and Yusop, M. 2008. Field Emission from a Single Carbon Nanofiber at Sub 100 nm Gap. Applied Physics Letters. 93(2): 023131. https://doi.org/10.1063/1.2959826

[20] Zamri, M., Ghosh, P., Wang, Z. P., Kawagishi, M., Hayashi, A., Hayashi, Y. and Tanemura, M. 2010. Direct Growth of Carbon Nanofibers on Metal Mesh Substrates by Ion Irradiation Method. Journal of Vacuum Science & Technology B. 28(2): C2C9-C2C12. https://doi.org/10.1116/1.3318694

[21] Azizir-Rahim, M., Yusop, M. Z. M., Othman, M. H. D., Ibrahim, M. and Tanemura, M. 2019. In Situ Transmission Electron Microscope: Joule Heating Effect on Graphitization of Copper Incorporated Carbon Nanofiber. International Journal of Automotive and Mechanical Engineering. 16(3): 6931-6939. https://doi.org/10.15282/ijame.16.3.2019.08.0520

[22] Bullen, A. J., O'Hara, K. E., Cahill, D. G., Monteiro, O. and von Keudell, A. 2000. Thermal Conductivity of Amorphous Carbon Thin Films. Journal of Applied Physics. 88(11): 6317-6320. https://doi.org/10.1063/1.1314301

[23] Robertson, J. 2002. Diamond-like Amorphous Carbon. Materials Science and Engineering: R: Reports. 37(4-6): 129-281. https://doi.org/10.1016/S0927-796X(02)00005-0

[24] Bayer, B. C., Bosworth, D. A., Michaelis, F. B., Blume, R., Habler, G., Abart, R., Weatherup, R. S., Kidambi, P. R., Baumberg, J. J., Knop-Gericke, A., Schloegl, R., Baehtz, C.,

Barber, Z. H., Meyer, J. C. and Hofmann, S. 2016. In Situ Observations of Phase Transitions in Metastable Nickel (Carbide)/Carbon Nanocomposites. The Journal of Physical Chemistry C. 120(39): 22571-22584. https://doi.org/10.1021/acs.jpcc.6b01555

[25] Chai, Y., Hazeghi, A., Takei, K., Chen, H.-Y., Chan, P. C. H., Javey, A. and Wong, H.-S. P. 2010. Graphitic Interfacial Layer to Carbon Nanotube for Low Electrical Contact Resistance. 2010 International Electron Devices Meeting (IEDM). 9.2.1-9.2.4. https://doi.org/10.1109/IEDM.2010.5703327

[26] Ugarte, D. 1992. Curling and Closure of Graphitic Networks under Electron-beam Irradiation. Nature. 359(6397): 707-709. https://doi.org/10.1038/359707a0

[27] Egerton, R. F., Li, P. and Malac, M. 2004. Radiation Damage in the TEM and SEM. Micron. 35(6): 399-409. https://doi.org/10.1016/j.micron.2004.02.003

[28] Banhart, F. 1999. Irradiation Effects in Carbon Nanostructures. Reports on Progress in Physics. 62(8): 1181-1221. https://doi.org/10.1088/0034-4885/62/8/201

[29] Börrnert, F., Avdoshenko, S. M., Bachmatiuk, A., Ibrahim, I., Büchner, B., Cuniberti, G. and Rümmeli, M. H. 2012. Amorphous Carbon under 80 kV Electron Irradiation: A Means to Make or Break Graphene. Advanced Materials. 24(41): 5630-5635. https://doi.org/10.1002/adma.201202173

[30] Lim, S. C., Jang, J. H., Bae, D. J., Han, G. H., Lee, S., Yeo, I.-S. and Lee, Y. H. 2009. Contact Resistance between Metal and Carbon Nanotube Interconnects: Effect of Work Function and Wettability. Applied Physics Letters. 95(26): 264103. https://doi.org/10.1063/1.3255016

https://doi.org/10.31875/2409-9848.2026.13.10

© 2026 Yusop and Tanemura
This is an open-access article licensed under the terms of the Creative Commons Attribution License (http://creativecommons.org/licenses/by/4.0/), which permits unrestricted use, distribution, and reproduction in any medium, provided the work is properly cited.